Influence of the phonon-bottleneck effect and low-energy vibrational modes on the slow spin-phonon relaxation in Kramers-ions-based Cu(II) and Co(II) complexes with 4-amino-3,5-bis-(pyridin-2-yl)-1,2,4-triazole and dicyanamide.

Ivan Potočňák[a], Oleksandr Bukrynov[b], Andrii Kliuikov[c,d], Mariia Holub[c,e], Svitlana Vitushkina[b,f], Erika Samoľová[g], Erik Čižmár[c] and Lucia Váhovská*[h]

[a]P. J. Šafárik University in Košice, Faculty of Science, Institute of Chemistry, Department of Inorganic Chemistry, Moyzesova 11, SK-041 54 Košice, Slovakia.

[b]V. N. Karazin Kharkiv National University, Faculty of Chemistry, Department of Applied Chemistry, Svobody sq. 4, UA-61022 Kharkiv, Ukraine.

[c]P.J. Šafárik University in Košice, Faculty of Science, Institute of Physics, Park Angelinum 9, SK-041 54 Košice, Slovakia.

[d]Slovak Metrological Institute, Karloveská 63, 842 55 Bratislava, Slovakia

[e]Synchrotron SOLEIL, L'Orme des Merisiers, Départementale 128, 91190 Saint-Aubin, France

[f]Institute of Experimental Physics of the Slovak Academy of Sciences, Department of Materials Physics, Watsonova 47, SK-040 01 Košice, Slovakia.

[g]Institute of Physics of the Czech Academy of Sciences, Na Slovance 2, 182 21 Prague 8, Czech Republic.

[b]University of Veterinary Medicine and Pharmacy in Košice, Department of Chemistry, Biochemistry and Biophysics, Komenského 73, SK-041 84 Košice, Slovakia.

Table S1 Crystal data and structure refinement for **1** and **2**.

Compound	**1**	**2**
Empirical formula	$CuC_{28}H_{20}N_{18}$	$CoC_{28}H_{20}N_{18}$
Formula weight	672.16	667.55
Temperature [K]	120(2)	95(2)
Wavelength [Å]	0.71073	1.54184
Crystal system	Triclinic	Triclinic
Space group	*P*-1	*P*-1
Unit cell dimensions [Å, °]	$a = 8.1722(3)$ $b = 9.1044(3)$ $c = 10.0931(4)$ $\alpha = 91.450(3)$ $\beta = 113.458(3)$ $\gamma = 96.047(3)$	$a = 13.4607(2)$ $b = 15.9166(2)$ $c = 21.7242(3)$ $\alpha = 83.175(1)$ $\beta = 73.697(1)$ $\gamma = 75.306(1)$
Volume [Å^3]	683.19(5)	4315.44(11)
Z	1	6
Calculated density [g.cm^{-3}]	1.634	1.541
Absorption coefficient [mm^{-1}]	0.859	5.150
F(000)	343	2046
Crystal shape, colour	Prism, turquoise	Prism, orange-brown
Crystal size [mm^3]	0.485 x 0.268 x 0.257	0.302 x 0.099 x 0.063
θ range for data collection [°]	3.322 – 26.50	2.874 – 76.345
Index ranges	$-10 \leq h \leq 10$ $-11 \leq k \leq 11$ $-12 \leq l \leq 12$	$-16 \leq h \leq 16$ $-20 \leq k \leq 19$ $-27 \leq l \leq 27$
Reflections collected	9544	79163
Independent reflections	2823 [$R_{\text{int}} = 0.0236$]	17767 [$R_{\text{int}} = 0.0253$]
T_{min}, T_{max}	0.740; 0.827	0.319, 1.000
Data/restraints/parameters	2823/0/222	17767/0/ 1341
Goodness-of-fit on F^2	1.079	1.054
Final *R* indices [$I > 2\sigma(I)$]	$R_1 = 0.0238$ $wR_2 = 0.0615$	$R_1 = 0.0350$ $wR_2 = 0.0974$
R indices (all data)	$R_1 = 0.0246$ $wR_2 = 0.0619$	$R_1 = 0.0431$ $wR_2 = 0.1030$
Largest diff. peak and hole [e.A^{-3}]	0.267 and -0.404	0.522 and -0.418

Table S2 Structural deformation of coordination polyhedra in **1** and **2.**

Structure [ML6]	**Σ**	**HP-6**	**PPY-6**	**OC-6**	**TPR-6**	**JPPY-6**
1	50.84°	28.941	27.592	1.362	16.741	29.908
2 (Co1)	56.60°	28.215	27.945	0.877	15.888	30.844
2 (Co2)	59.28°	27.937	27.981	0.883	15.873	30.966
2 (Co3)	62.57°	27.590	27.533	0.886	15.492	30.457
2 (Co4)	56.98°	28.197	27.874	0.865	15.686	30.856

HP-6	1 D6h	Hexagon
PPY-6	2 C5v	Pentagonal pyramid
OC-6	3 Oh	Octahedron
TPR-6	4 D3h	Trigonal prism
JPPY-6	5 C5v	Johnson pentagonal pyramid J2

$\sum = \sum_{1}^{12}(|\varphi_i - 90|)$; where φi is value of the N-M-N octahedron angle

Table S3 Selected bond distances (Å) for **2** (Co2–Co4).

Bond distances	**2** (Co2) x = 1	**2** (Co3) x = 2, y = 3	**2** (Co4) x = 4, y = 5
M–N2x	2.109(1)	2.099(1)	2.096(1)
M–N6x	2.147(1)	2.145(1)	2.149(1)
M–N8x	2.093(1)	2.105(1)	2.106(1)
M–N2y	-	2.103(1)	2.092(1)
M–N6y	-	2.145(1)	2.148(1)
M–N8y	-	2.097(1)	2.116(1)
N8x–C8x	1.159(2)	1.156(2)	1.149(2)
C8x–N7x	1.301(2)	1.312(2)	A 1.317(4) B 1.348(6)
N7x–C9x	1.290(2)	1.292(2)	A 1.364(6) B 1.305(7)
C9x–N9x	1.164(2)	1.171(2)	1.147(3)
N8y–C8y	-	1.147(2)	1.159(2)
C8y–N7y	-	1.304(2)	A 1.303(3) B 1.373(15)
N7y–C9y	-	1.325(2)	A 1.337(4) B 1.26(2)

C9y–N9y	-	1.142(3)	1.151(3)

Table S4 Selected bond angles (°) for **2** (Co2–Co4).

Bond angles	**2** (Co2) x = 1	**2** (Co3) x = 2, y = 3	**2** (Co4) x = 4, y = 5
N2x–M–N6x	76.99(5)	77.04(5)	77.02(5)
N2x–M–N8x	89.35(5)	91.66(5)	90.05(5)
N6x–M–N8x	91.16(5)	89.68(5)	90.51(5)
N2x–M–N8x^{v}	90.65(5)	-	-
N2x–M–N6x^{v}	103.01(5)	-	-
N6x–M–N8x^{v}	88.84(5)	-	-
N2x–M–N2y	-	179.02(5)	179.40(5)
N2x–M–N6y	-	102.27(5)	103.10(5)
N2x–M–N8y	-	88.73(5)	90.99(5)
N6x–M–N2y	-	103.43(5)	102.72(5)
N6x–M–N6y	-	177.50(5)	179.40(4)
N6x–M–N8y	-	90.76(5)	88.86(5)
N8x–M–N2y	-	89.21(5)	90.49(5)
N8x–M–N6y	-	92.75(5)	90.08(5)
N8x–M–N8y	-	179.47(5)	178.63(5)
N2y–M–N6y	-	77.22(5)	77.16(5)
N2y–M–N8y	-	90.40(5)	88.47(5)
N6y–M–N8y	-	86.82(5)	90.55(5)
N8x–C8x–N7x	170.3(2)	173.2(2)	A 163.6(5) B 159.6(7)
C8x–N7x–C9x	123.0(2)	121.0(2)	A 118.1(5) B 120.2(7)
N7x–C9x–N9x	172.9(2)	175.3(2)	A 164.5(5) B 159.9(7)
N8y–C8y–N7y	-	173.2(2)	A 170.1(3) B 150.9(19)
C8y–N7y–C9y	-	118.7(2)	A 121.3(3) B 122(2)
N7y–C9y–N9y	-	174.5(2)	A 164.5(5) B 159.9(7)

[Symmetry code: (v) = $1 - x$, $1 - y$, $- z$]

Table S5 Cg···Cg distances and angles (Å, °) characterizing π–π interactions in **1** and **2**.

Compound	Cg(I)···Cg(J)	Cg···Cg	α [a]	β	γ
1	Cg1···Cg2^{ii}	3.5517(9)	3.92(7)	24.3	21.2
	Cg1···Cg1^{iii}	3.5089(9)	0.00(7)	19.9	19.9
2	Cg1···Cg12	3.6051(10)	3.91(8)	23.5	21.0
	Cg2···Cg10	3.6094(10)	4.01(8)	20.1	22.8
	Cg3···Cg7^{ii}	3.7329(9)	5.85(8)	24.1	21.2
	Cg4···Cg5^{ii}	3.7422(9)	9.20(8)	20.4	27.9
	Cg6···Cg8^{iii}	3.6592(9)	8.29(8)	22.3	19.0
	Cg9···Cg11^{iv}	3.5710(10)	5.43(8)	22.3	17.9

[Symmetry codes: (ii) = 1 – *x*, 1 – *y*, 1 – *z*; (iii) = 2 – *x*, 1 – *y*, 2 – *z* (**1**);

(ii) = *x* – 1, *y*, *z*; (iii) = 1 – *x*, 1 – *y*, 1 – *z*; (iv) = 2 – *x*, – *y*, 1 – *z* (**2**)]

Cg1 represents centroid of the uncoordinated pyridyl ring containing N5 atom

Cg2 represents centroid of the coordinated pyridyl ring containing N6 atom

Cg3 represents centroid of the uncoordinated pyridyl ring containing N51 atom

Cg4 represents centroid of the coordinated pyridyl ring containing N61 atom

Cg5 represents centroid of the uncoordinated pyridyl ring containing N52 atom

Cg6 represents centroid of the uncoordinated pyridyl ring containing N53 atom

Cg7 represents centroid of the coordinated pyridyl ring containing N62 atom

Cg8 represents centroid of the coordinated pyridyl ring containing N63 atom

Cg9 represents centroid of the uncoordinated pyridyl ring containing N54 atom

Cg10 represents centroid of the uncoordinated pyridyl ring containing N55 atom

Cg11 represents centroid of the coordinated pyridyl ring containing N64 atom

Cg12 represents centroid of the coordinated pyridyl ring containing N65 atom

[a] α is the dihedral angle between planes I and J. β is the angle between Cg(I)···Cg(J) vector and normal to plane I. γ is the angle between Cg(I)···Cg(J) vector and normal to plane J

Table S6 Inter- and intramolecular N–H···N hydrogen bond interactions in **1** and **2** (Å, °)

Compound	Donor–H···Acceptor	D–H	H···A	D···A	< D–H···A
1	N3–H1N3···N9^{iv}	0.90(2)	2.22(2)	2.986(2)	143(2)
(intra)	N3–H2N3···N5	0.87(2)	2.19(2)	2.902(2)	140(2)
2	N3–H3A···N94^{ii}	0.86(2)	2.10(2)	2.9164(1)	159(2)
	N31–H31B···N93^{v}	0.90(2)	2.13(2)	2.9364(1)	148(2)
	N32–H32B···N92^{vi}	0.92(2)	2.05(2)	2.9188(1)	159(2)
	N33–H33B···N91^{iii}	0.93(2)	2.39(2)	3.0600(1)	129(2)
	N33–H33B···N92^{iii}	0.93(2)	2.58(3)	3.2228(1)	126(2)
	N34–H34A···N95^{vii}	0.87(2)	2.10(2)	2.9132(1)	155(2)
	N35–H35B···N9^{viii}	0.88(2)	2.09(2)	2.9195(1)	157(2)
(intra)	N3–H3B···N5	0.92(2)	2.05(2)	2.8347(1)	143(2)
	N31–H31A···N51	0.97(2)	1.99(2)	2.8194(1)	142(2)
	N32–H32A···N52	0.93(2)	2.01(2)	2.8124(1)	143(2)
	N33–H33A···N53	0.95(2)	2.02(2)	2.8182(1)	140(2)
	N34–H34B···N54	0.90(2)	2.08(2)	2.8475(1)	142(2)
	N35–H35A···N55	0.90(2)	2.06(2)	2.8467(1)	146(2)

[Symmetry codes: (iv) = $1-x, -y, -z$ (**1**); (v) = $1-x, 1-y, -z$; (vi) = $2-x, 1-y, 1-z$; (vii) = $1-x, -y, 1-z$ (viii) = $2-x, -y, -z$ (**2**)]

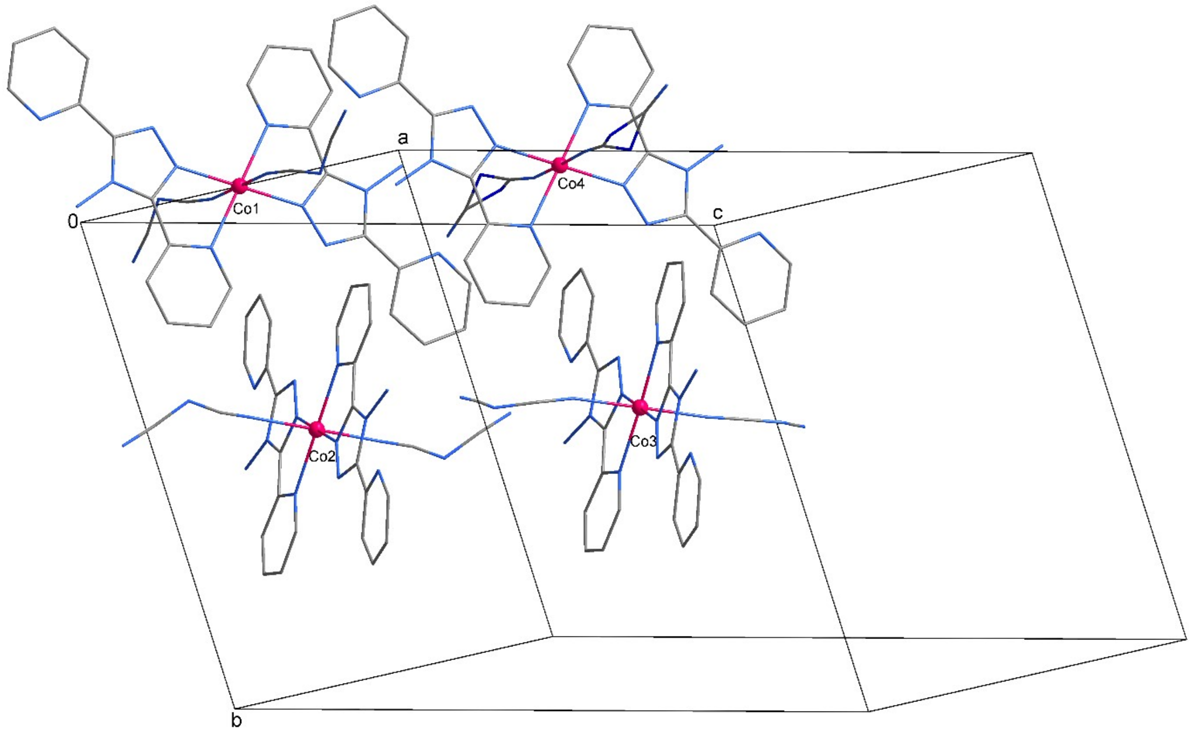

Fig. S1: Mutual position of Co1 – Co4 molecules in the unit cell of **2** (hydrogen atoms are omitted for clarity).

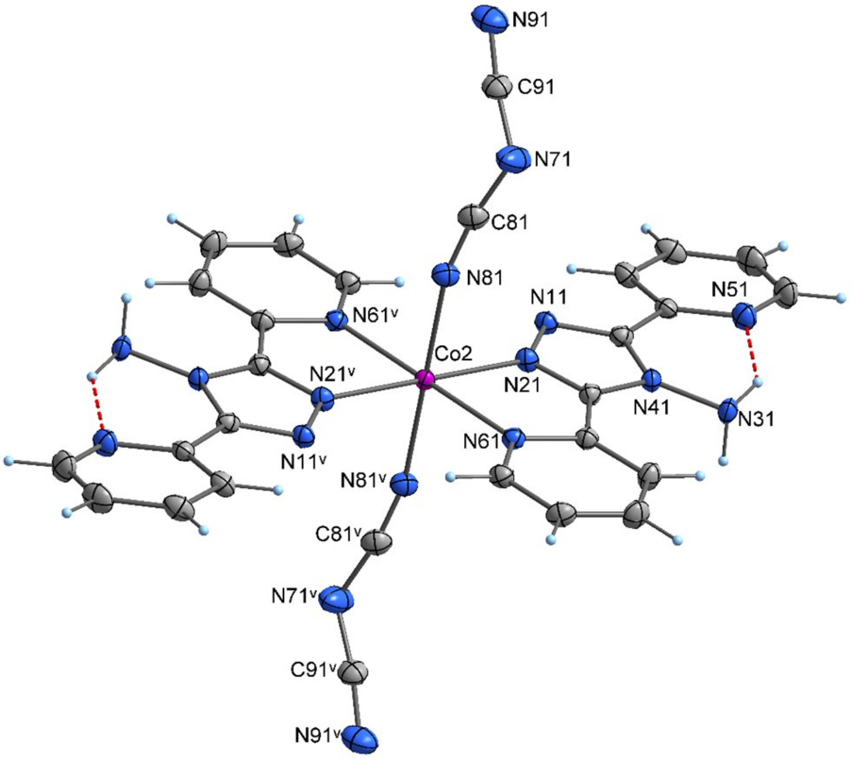

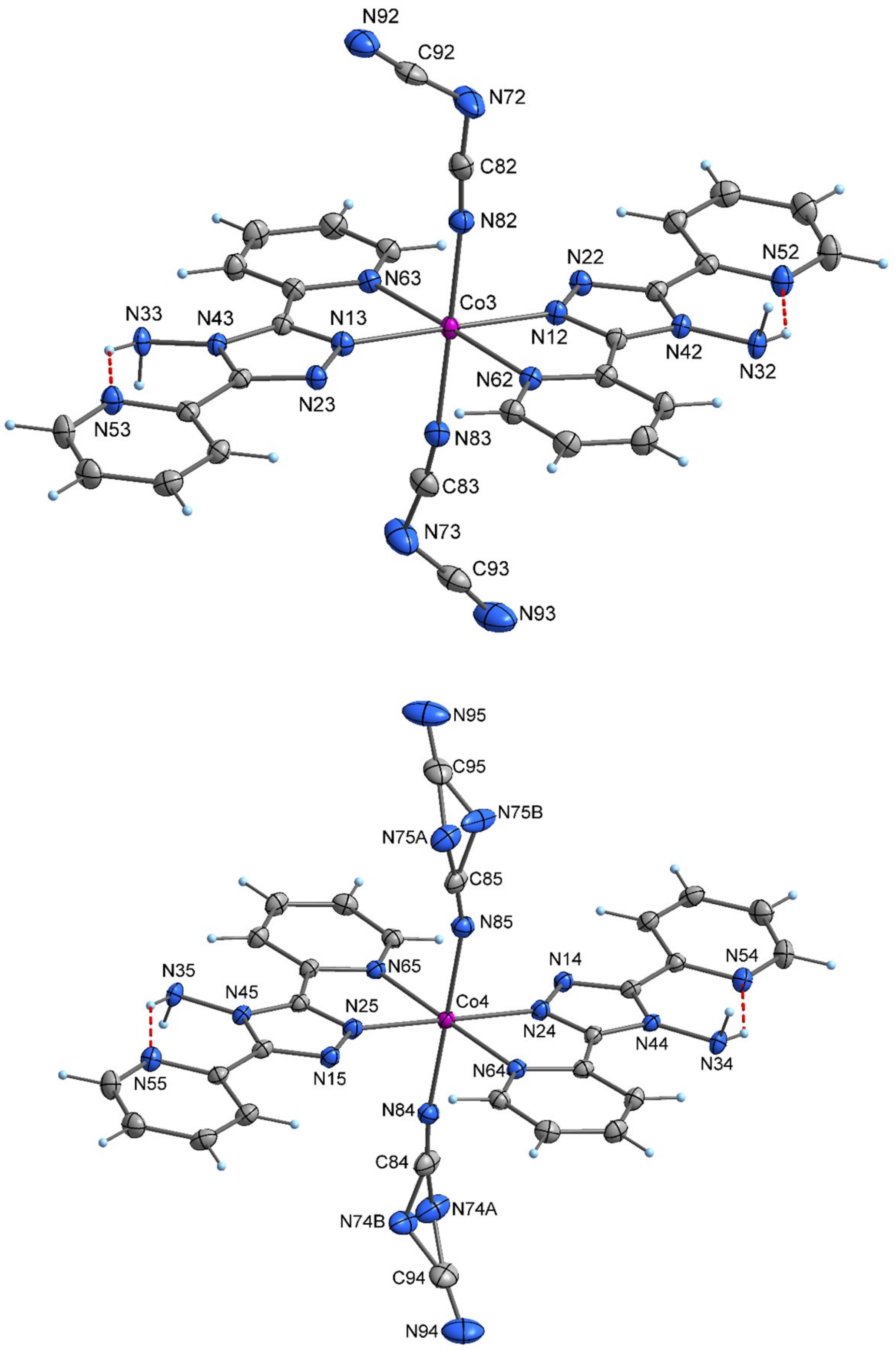

Fig. S2: Molecular structure of Co2 – Co4 molecules in **2** with displacement ellipsoids (50% probability) and intramolecular hydrogen bonds (dashed red lines). [Symmetry code: v = 1 – *x*, 1 – *y*, – *z*]

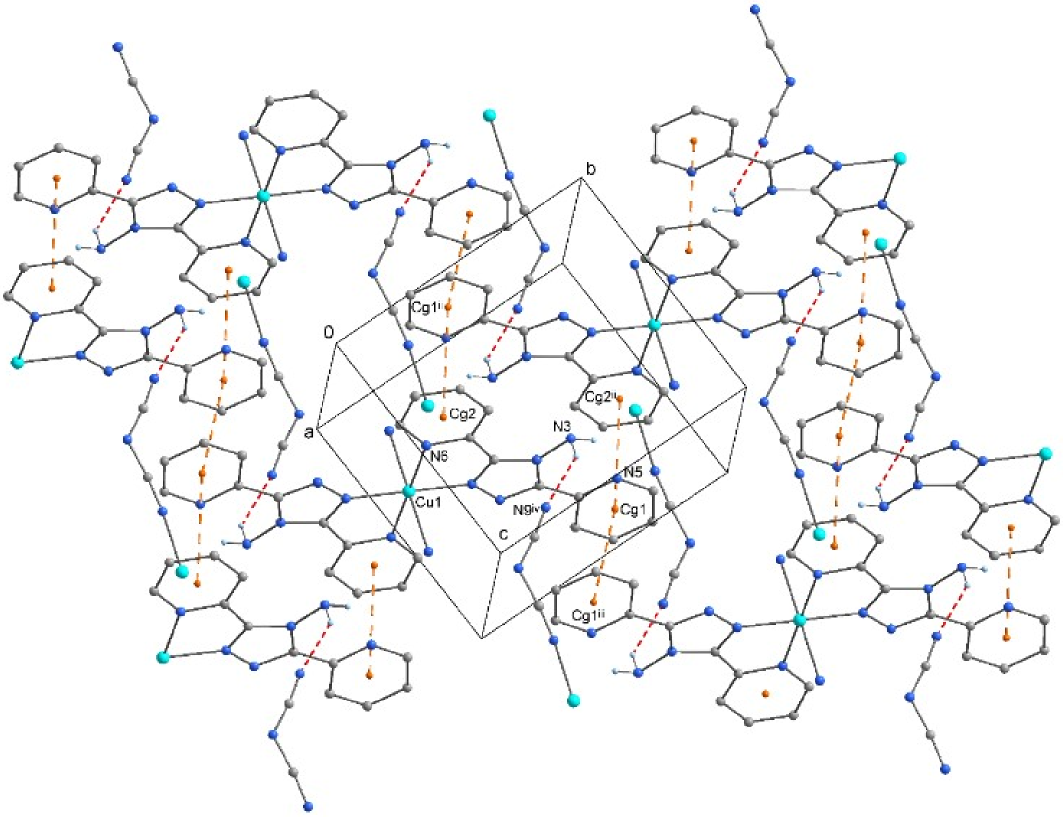

Fig. S3 π-π interactions (orange dashed lines) between pyridyl rings and intermolecular hydrogen bonds (red dashed lines) in **1**. Hydrogen atoms not involved in the hydrogen bonds are omitted for clarity. [Symmetry codes: (ii) = $1 - x, 1 - y, 1 - z$; (iii) = $2 - x, 1 - y, 2 - z$; (iv) = $1 - x, - y, - z$].

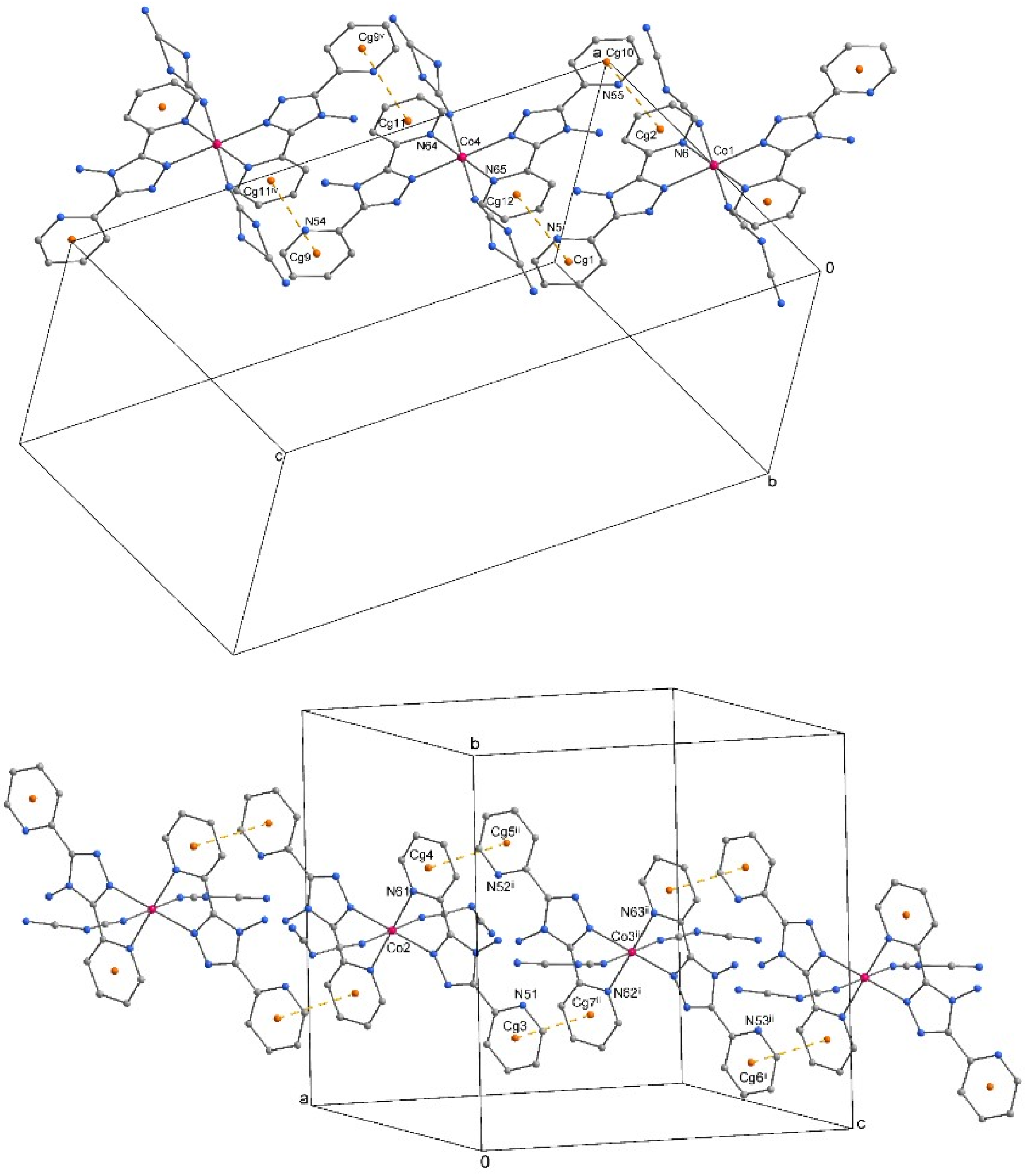

Fig. S4 π-π interactions (orange dashed lines) in **2** between pyridyl rings involving Co1 and Co4 units (up), and Co2 and Co3 units (down). Hydrogen atoms and dca ligands are omitted for clarity. [Symmetry codes: (ii) = $x - 1$, y, z; (iii) = $1 - x$, $1 - y$, $1 - z$; (iv) = $2 - x$, $- y$, $1 - z$].

Analysis of the slow magnetic relaxation

The extraction of the relaxation times was performed using a modified Debye model accounting for two independent relaxation processes given by the formula

$$\chi(\omega) = \chi_S + \sum_{k=1}^{K} \frac{\chi_{Tk} - \chi_{Tk-1}}{1 + \left(i\omega\tau_k\right)^{1-\alpha_k}} , \qquad \textbf{(ES1)}$$

where χ_S is the overall adiabatic susceptibility, χ_{Tk} is the isothermal susceptibility, $\omega = 2\pi f$ is the angular frequency, τ_k is the relaxation time for *k*-th relaxation process, α_k describes the distribution of relaxation times of *k*-th relaxation process, and *K* defines the number of relaxation channels. The real and the imaginary parts of **Eq. ES1** were extracted by a fitting script in MATLAB and fitted to the experimental data of $\chi^{'}$ and $\chi^{''}$ simultaneously.

A complete formula that would include all possible relaxation mechanisms (field-dependent Raman described by Brons-Van Vleck model, direct, Orbach, and QTM process) coexisting in one relaxation channel can be written as

$$\tau^{-1} = \tau_{BVV}^{-1} + \tau_{D}^{-1} + \tau_{ORB}^{-1} + \tau_{QTM}^{-1} = d\frac{1 + eB^2}{1 + fB^2} + ATB^4 + \tau_0^{-1} e^{-\frac{U_{eff}}{k_B T}} + \frac{D_1}{1 + D_2 B^2}, \qquad \textbf{(ES2)}$$

where *d* represents a zero-field Raman process $\tau_{ZF}^{-1} \equiv \tau_{R}^{-1} = CT^n$, with characteristic constants A, C, D_1, D_2, e, f, τ_0, and U_{eff} for each process.

Magnetic properties of 1

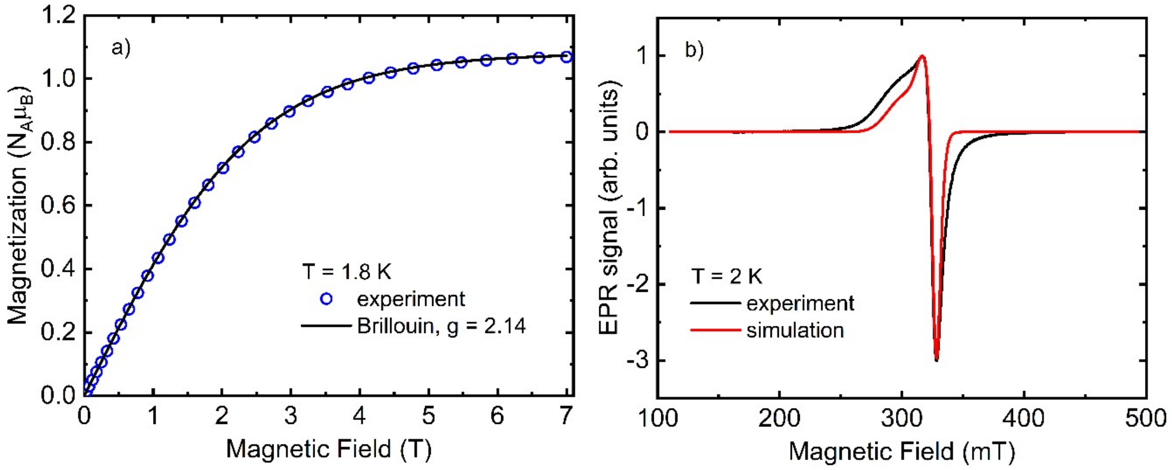

Fig. S5 a) The field dependence of the magnetization of **1** measured at 1.8 K (symbols), including a fit by the Brillouin function (solid line). b) X-band EPR spectra of **1** at 2 K (black solid line) including a simulation with $[g_x, g_y, g_z]$ = [2.060, 2.075, 2.270] and anisotropic line broadening $[\Delta B_x, \Delta B_y, \Delta B_z]$ = [6.0, 17.8, 34.6] mT (red solid line).

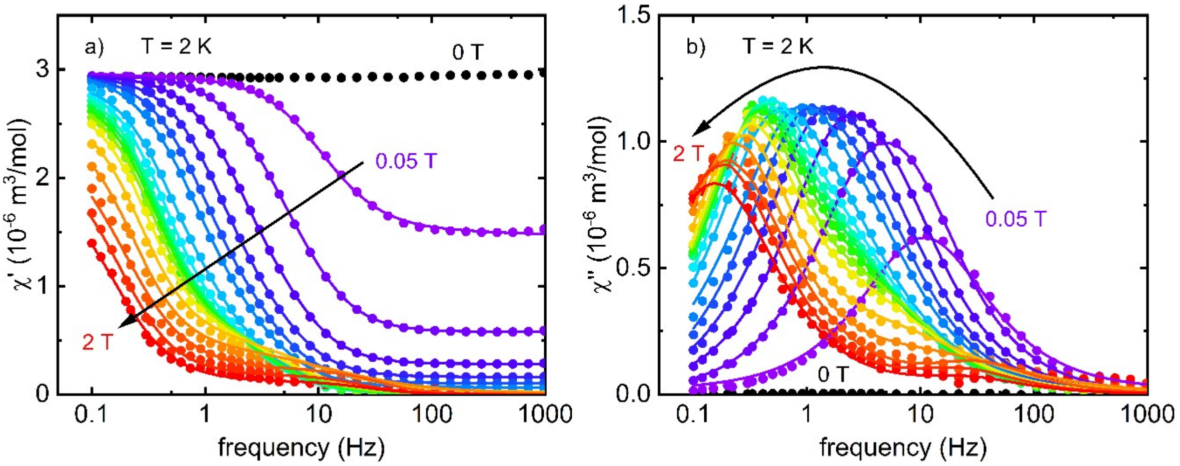

Fig. S6 Frequency dependences of χ' (a) and χ'' (b) of a nascent sample of **1** obtained at 2 K at various static magnetic fields (symbols), including the fits (solid lines of corresponding color) using the modified Debye model Eq. ES1.

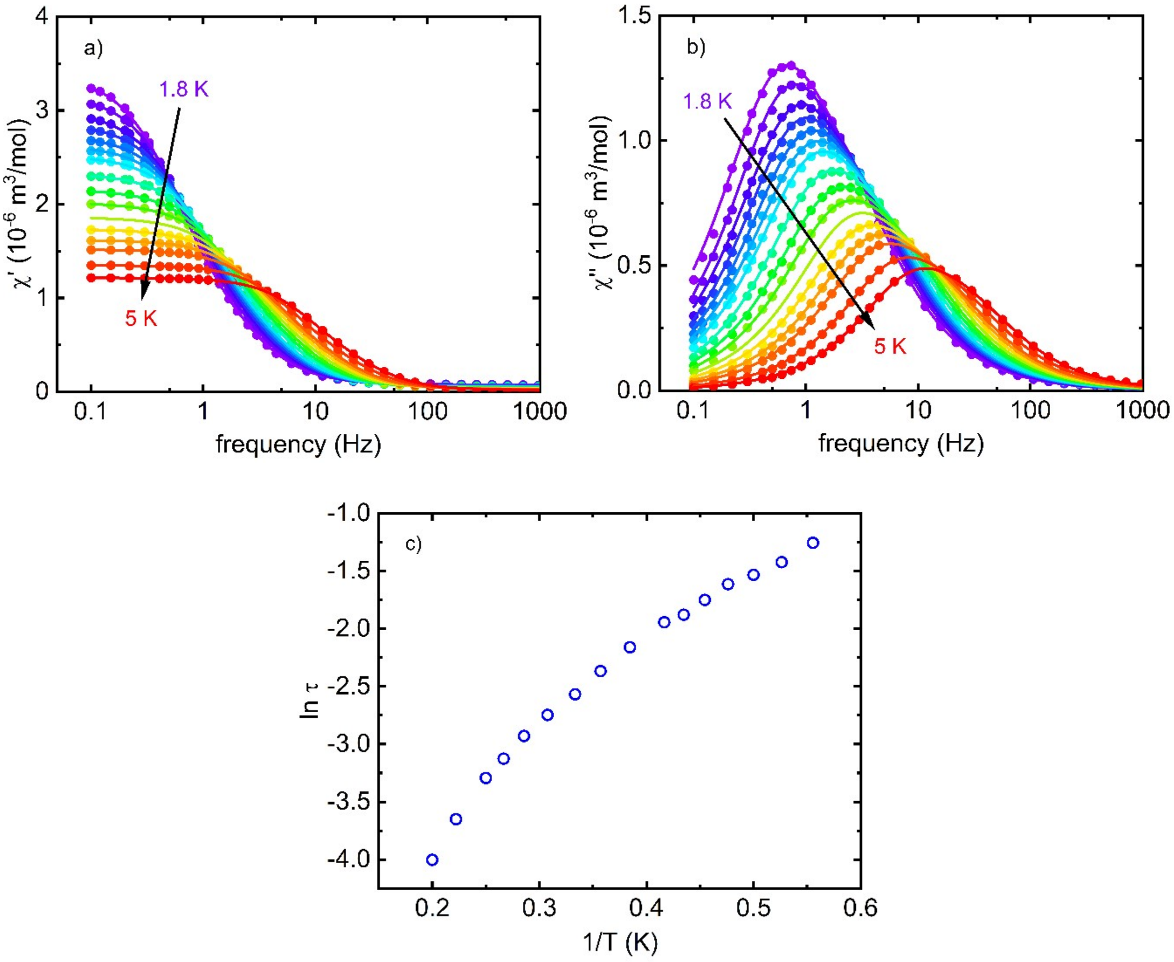

Fig. S7 Frequency dependences of χ' (a) and χ'' (b) of a nascent sample of **1** obtained at 0.3 T (symbols) at various temperatures, including the fits (solid lines of corresponding color) using the modified Debye model Eq. ES1. Arrhenius plot ($ln\tau \propto T^{-1}$) obtained from the analysis using the modified Debye model (c).

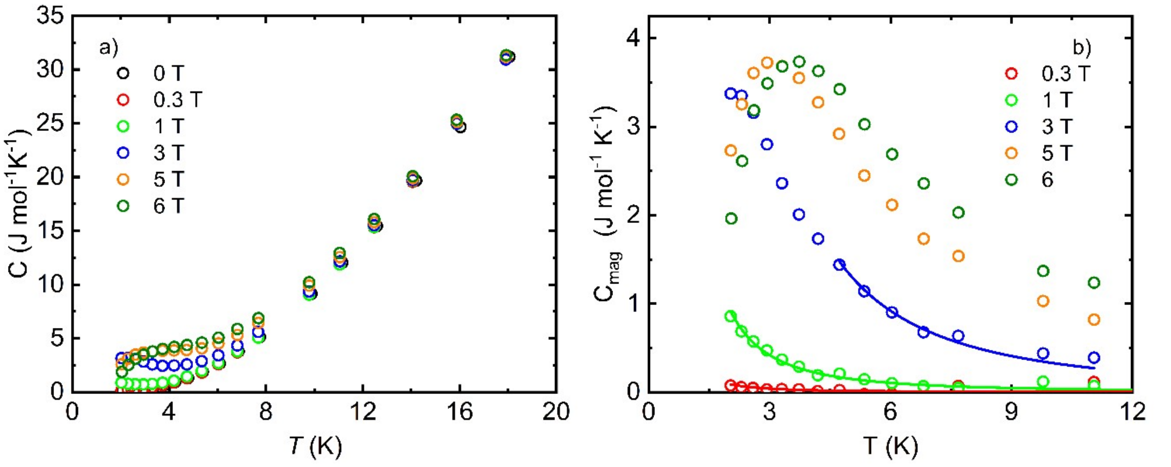

Fig. S8 a) Temperature dependence of total specific heat of **1** in magnetic field. b) Magnetic specific heat C_{mag} (open symbols), solid lines represent T^{-2} behaviour.

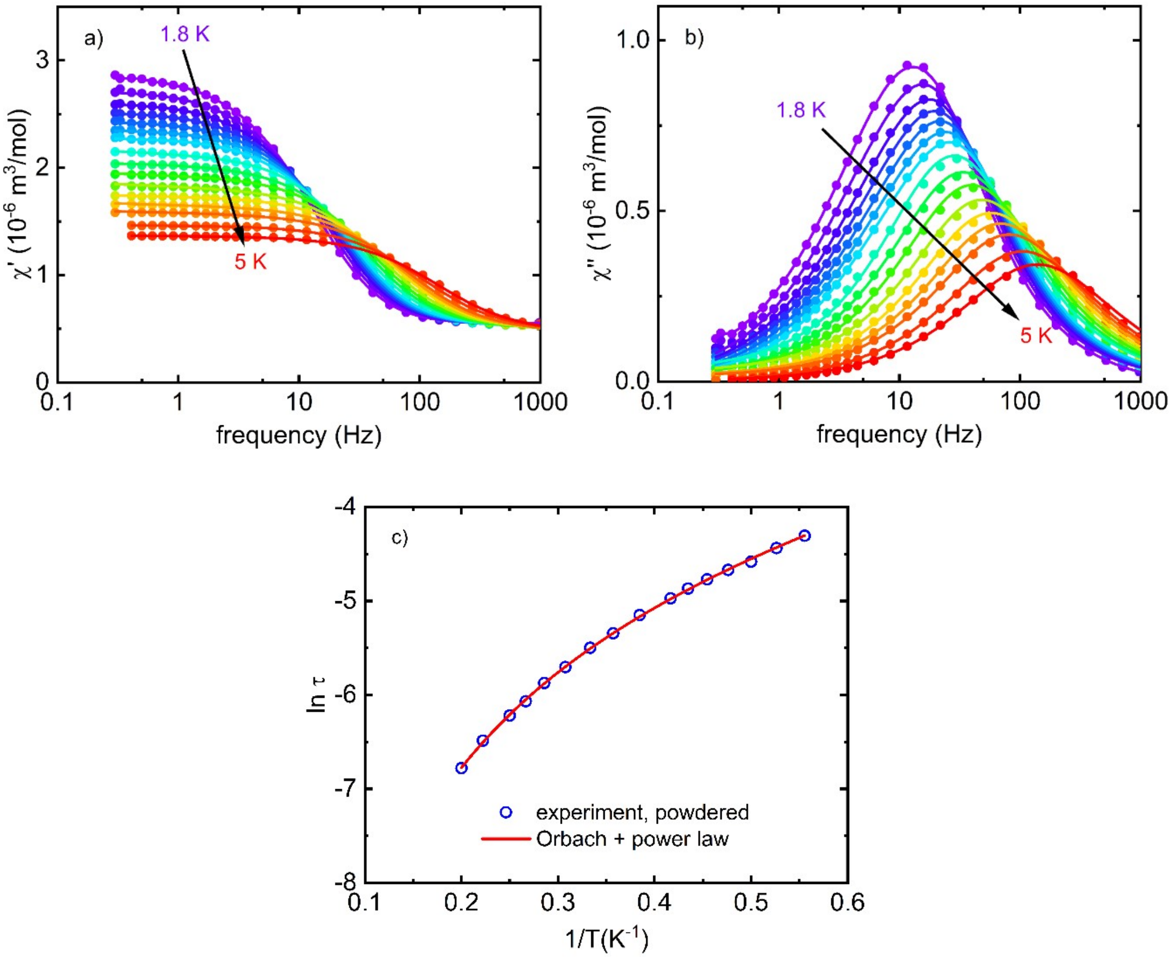

Fig. S9 Frequency dependences of χ' (a) and χ'' (b) of a powdered sample of **1** obtained at 0.3 T at various temperatures (symbols) including the fits (solid lines of corresponding color) using the modified Debye model Eq. ES1. Arrhenius plot ($\ln \tau \propto T^{-1}$) obtained from the analysis using the modified Debye model includes the fit of Eq. 4 assuming Orbach and power law contribution (c).

Table S7 Best-fit parameters of the Brons-van Vleck model, Eq. 3, used to reproduce the field dependence of the relaxation time of a powdered sample of **1** at different temperatures.

T (K)	c ($T^{-4}s^{-1}$)	d (s^{-1})	e (T^{-2})	f (T^{-2})
1.8	13.2	239.5	18.3	112.6
2	12.6	324.3	17.7	107.7
2.5	13.3	472.5	16.7	100.7
3	13.7	688.3	15.2	89.4
3.5	14.3	904.1	12.9	69.7
4	12	1206	13.2	68.8
5	13.8	1673.6	10.1	40.2
6	13.5	2180.3	9	32

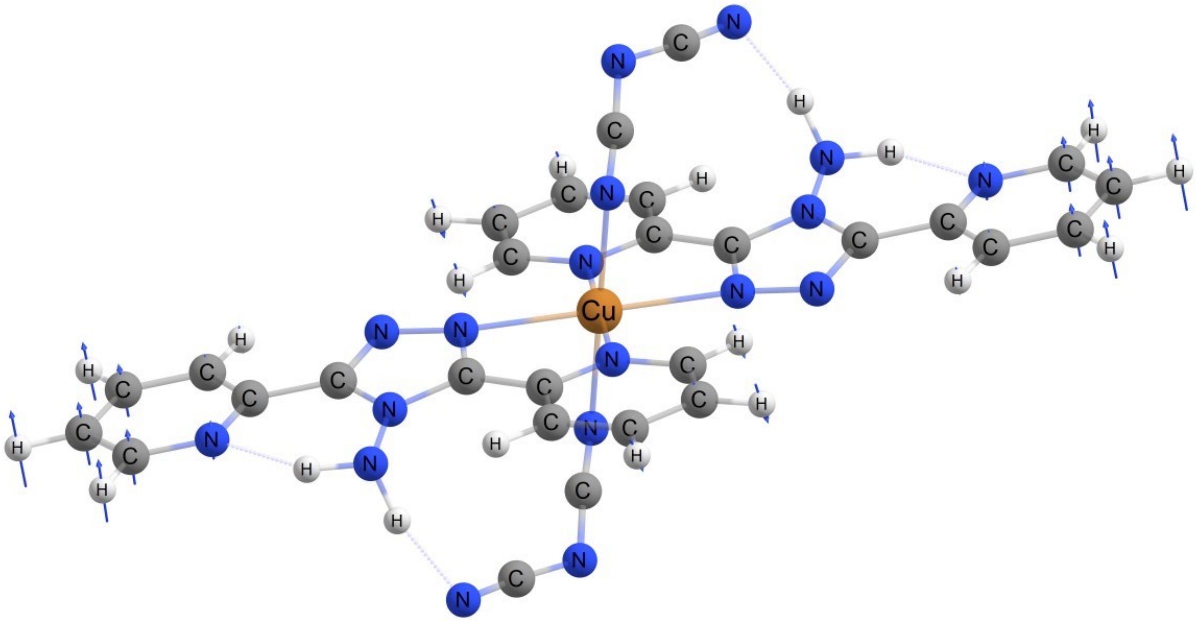

Fig. S10 The lowest energy (10.77 cm^{-1}) vibrational mode in the molecule of **1**, geometry optimized in the gas phase, calculated by ORCA. Blue arrows show the displacement vectors, plotted using Chemcraft - graphical software for visualization of quantum chemistry computations. https://www.chemcraftprog.com.

Magnetic properties of 1

Table S8 Effective *g*-factors of the ground Kramers doublet for **1** derived from SA-CASSCF/NEVPT2 calculations in ORCA, assignment of Co(II) ions as in Figs. 1 and S2.

	g_1	g_2	g_3
Co1	1.52	2.20	7.18
Co2	1.52	2.25	6.99
Co3	1.42	1.98	6.98
Co4	1.53	2.24	7.17

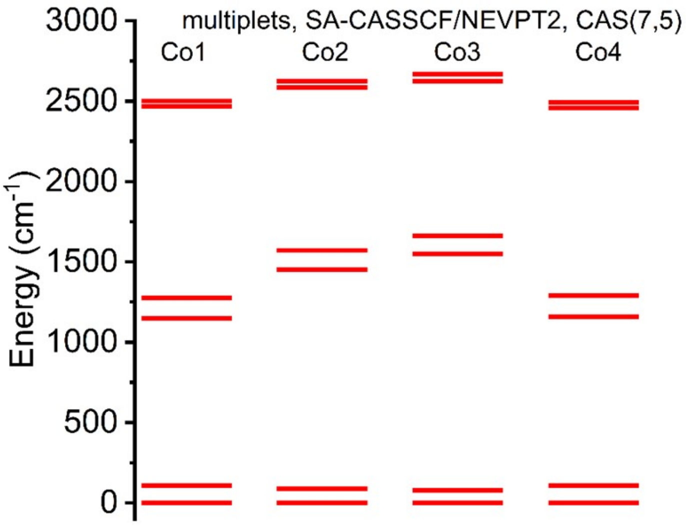

Fig. S11 The energies of 6 lowest multiplets as obtained from SA-CASSCF/NEVPT2 for **2**.

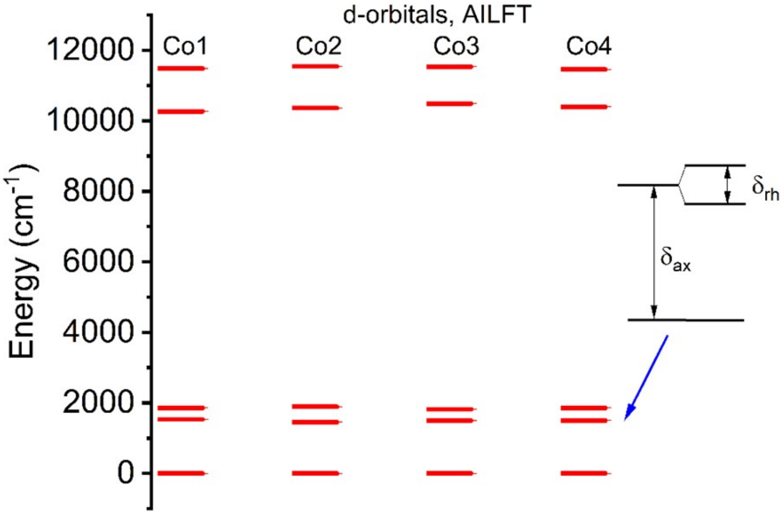

Fig. S12 The energies of *d*-orbitals of **2** obtained from AILFT analysis.

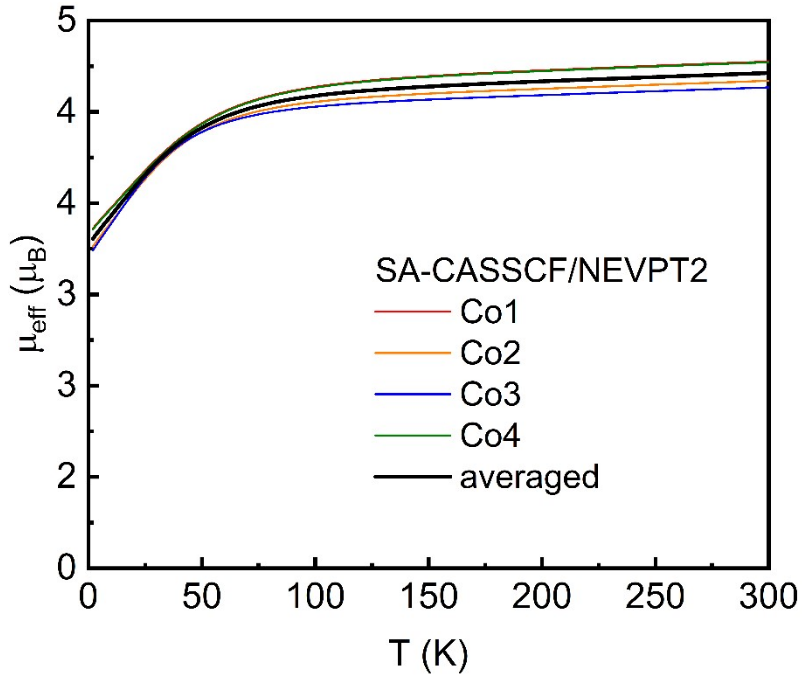

Fig. S13 The individual contributions of four nonequivalent Co(II) sites to μ_B as obtained by ORCA.

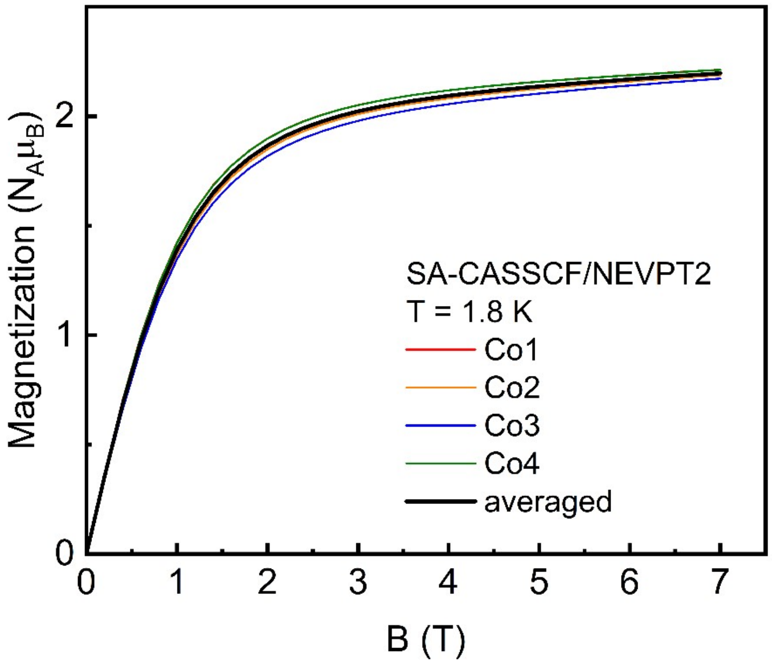

Fig. S14 The individual contributions of four nonequivalent Co(II) sites to magnetization at 1.8 K as obtained by ORCA.

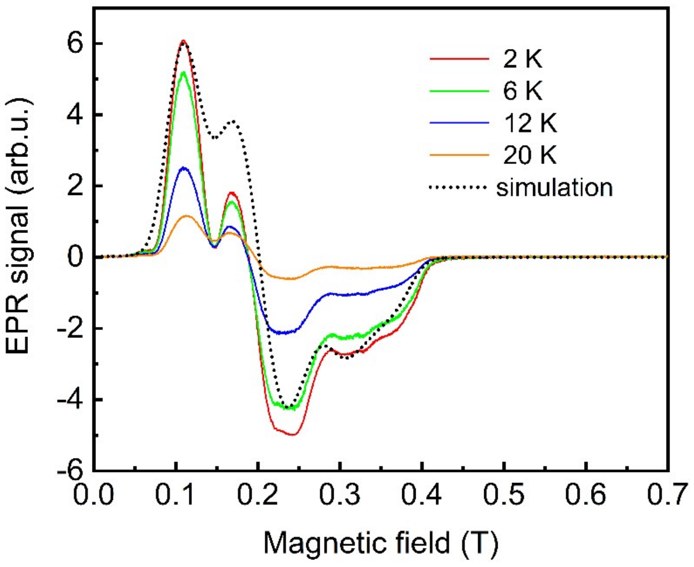

Fig. S15 X-band EPR spectra of **2** obtained at low temperatures.

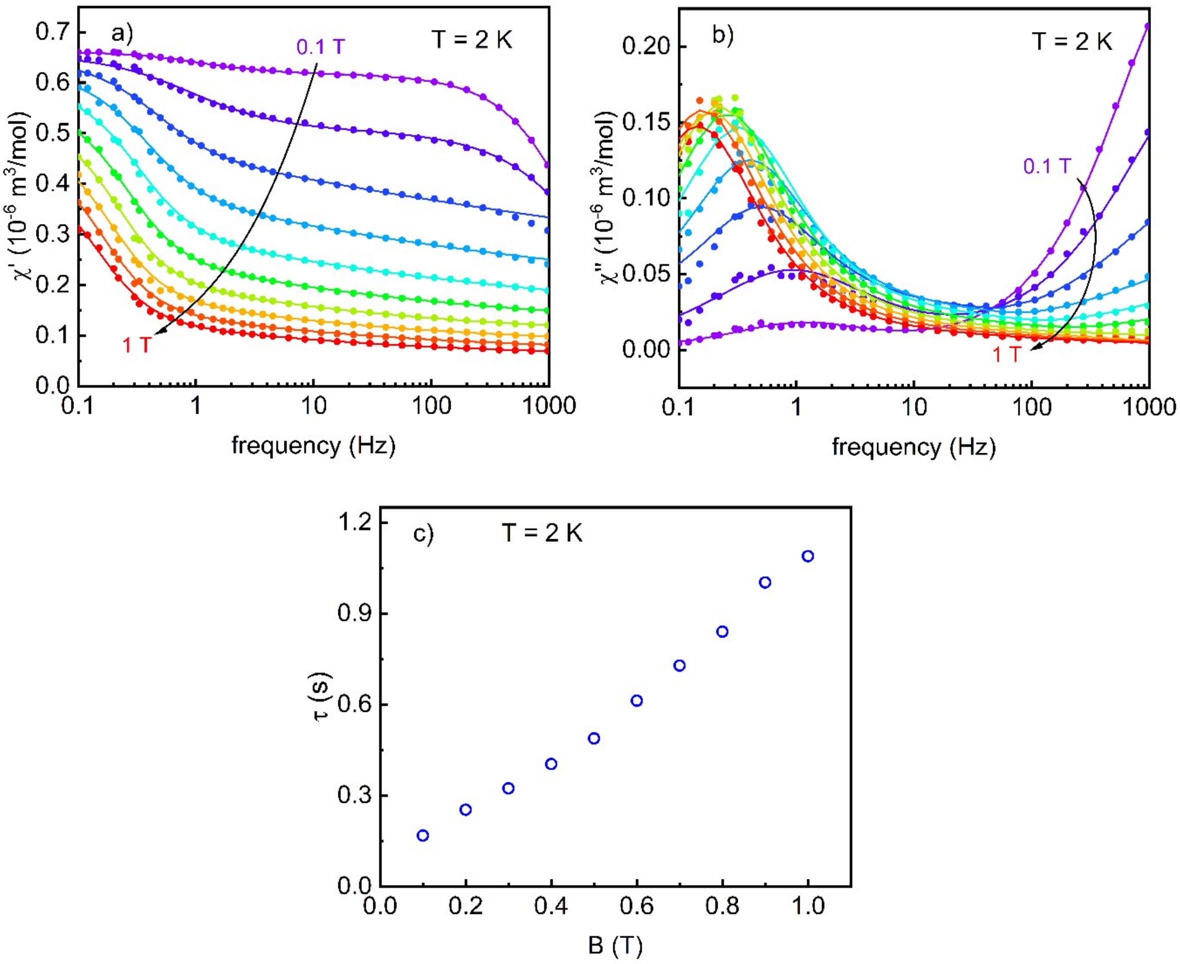

Fig. S16 Frequency dependences of χ' (a) and χ'' (b) of a powdered sample of **2** obtained at 2 K at various static magnetic fields (symbols), including the fits (solid lines of corresponding color) using the modified Debye model Eq. ES1 with two relaxation channels to extract the field dependence of relaxation time for the low-frequency relaxation channel (c).

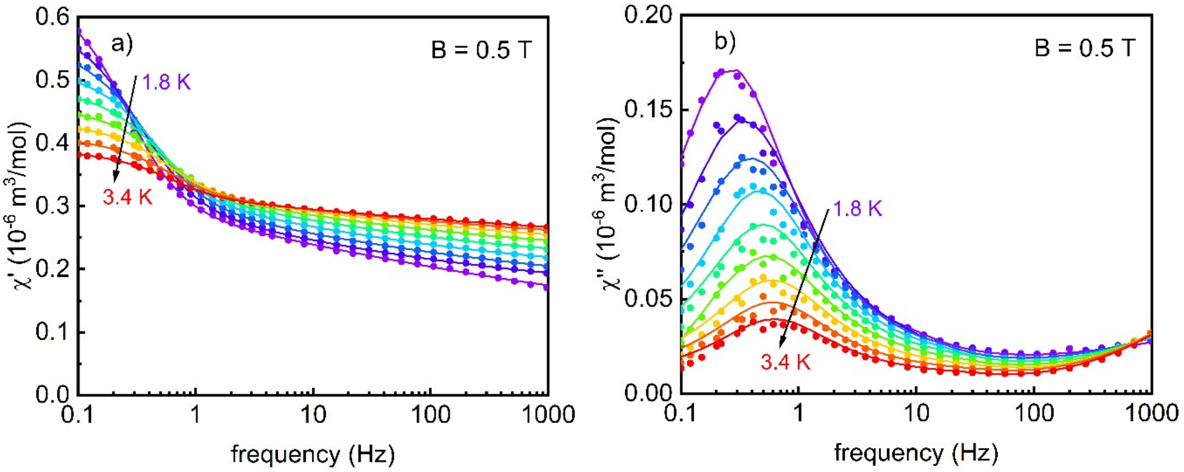

Fig. S17 Frequency dependences of χ' (a) and χ'' (b) of a powdered sample of **2** obtained in 0.5 T at various temperatures (symbols) including the fits (solid lines of corresponding color) using the modified Debye model Eq. ES1.